Matrix architecture defines the preferential localization and migration of T cells into the stroma of human lung tumors

Hélène Salmon,[1,2] Katarzyna Franciszkiewicz,[3] Diane Damotte,[4,5,6,7] Marie-Caroline Dieu-Nosjean,[4,5,6] Pierre Validire,[4,5,6,8] Alain Trautmann,[1,2] Fathia Mami-Chouaib,[3] and Emmanuel Donnadieu[1,2]

[1]Institut Cochin, Université Paris Descartes, CNRS (UMR 8104), Paris, France. [2]INSERM U1016, Paris, France. [3]INSERM U753, Institut Gustave Roussy, Villejuif, France. [4]INSERM U872, Centre de Recherche des Cordeliers, Paris, France. [5]Université Pierre et Marie Curie (Paris 6), UMRS 872, Paris, France. [6]Université Paris Descartes, UMRS 872, Paris, France. [7]Service d'Anatomo-pathologie, Hôpital Hôtel Dieu, AP-HP, Paris, France. [8]Institut Mutualiste Montsouris, Paris, France.

Appropriate localization and migration of T cells is a prerequisite for antitumor immune surveillance. Studies using fixed tumor samples from human patients have shown that T cells accumulate more efficiently in the stroma than in tumor islets, but the mechanisms by which this occurs are unknown. By combining immunostaining and real-time imaging in viable slices of human lung tumors, we revealed that the density and the orientation of the stromal extracellular matrix likely play key roles in controlling the migration of T cells. Active T cell motility, dependent on chemokines but not on β1 or β2 integrins, was observed in loose fibronectin and collagen regions, whereas T cells migrated poorly in dense matrix areas. Aligned fibers in perivascular regions and around tumor epithelial cell regions dictated the migratory trajectory of T cells and restricted them from entering tumor islets. Consistently, matrix reduction with collagenase increased the ability of T cells to contact cancer cells. Thus, the stromal extracellular matrix influences antitumor immunity by controlling the positioning and migration of T cells. Understanding the mechanisms by which this collagen network is generated has the potential to aid in the development of new therapeutics.

Introduction

Cancer cells express antigens recognized by T cells and can therefore elicit specific antitumor immune response. However, tumors can escape immune control, and multiple mechanisms altering T cell functions have been described previously (1, 2). One major issue concerns the limited ability of T lymphocytes to interact with tumor cells: T cell entry into tumors is often limited, mostly due to a lack of adhesion molecules and to abnormal vessel structures (3, 4). An additional point that has received too little attention thus far concerns the localization of T cells within a tumor. If T cells and tumor cells are physically far apart, the chance of cell-cell interaction, as well as tumor rejection, drops considerably. Immunohistochemistry has revealed that in most human solid tumors, T cells are not randomly distributed (5–7). Instead, T lymphocytes are usually sparse in tumor islets and more concentrated in the stroma, a surrounding microenvironment composed of noncancer cells along with the ECM. Default in T cell infiltration might be a major obstacle to T cell–based immunotherapy for cancer, which underlines the importance of elucidating the mechanisms responsible for T cell distribution into human tumors.

The recent development of improved imaging approaches, such as 2-photon microscopy, has shed light on the mechanisms contributing to T cell localization and migration in murine secondary lymphoid organs, inflamed tissues, and tumors. A combination of external cues, including chemokines and structural determinants, are supposed to control the interstitial migration of T cells (8). For instance, in lymph nodes, T cell displacement is guided by fibroblastic reticular cells that secrete CCR7 ligands (9, 10). These environmental determinants also explain the segregation of B and T cells within B cell follicles and T cell zones, respectively.

According to these prior studies, the distribution of T cells in the tumor environment could be dictated by the presence of chemoattractants and other external cues in the stroma, rather than in the tumor cell region. In several human cancers, correlations have been established between the expression of intratumoral chemokines and the number of T lymphocytes found within the whole tumor (11, 12). These results, albeit important, do not prove the existence of a causal relationship between the presence of a chemokine and the recruitment of T cells. As for structural components that might guide T cells, fibrillar ECM, whose makeup includes type I collagen and fibronectin, is an important constituent of the stroma. Although these determinants have previously been shown to influence the functions and migration of cancer cells (13), it is not known whether they play a role in the localization and dynamic behavior of T cells in the tumor stroma. Finally, the limited infiltration of tumor nests could be explained by the presence of physical or chemical barriers. Therefore, direct observation of the distribution and motility of T cells in different regions of the tumor is needed in order to gain insights into possible obstacles for lymphocyte navigation.

In the present work, we studied the localization and migration of fluorescent T cells into viable slices of human lung tumors. We used a live cell imaging approach that was initially set up in murine lymph nodes and designed to identify factors involved in T cell positioning and migration into and within a tissue (9). Our results indicated that the tumor epithelial compartment is an unfavorable recruitment and migration region for T cells. In contrast, we

Conflict of interest: The authors have declared that no conflict of interest exists.
Citation for this article: *J Clin Invest.* 2012;122(3):899–910. doi:10.1172/JCI45817.

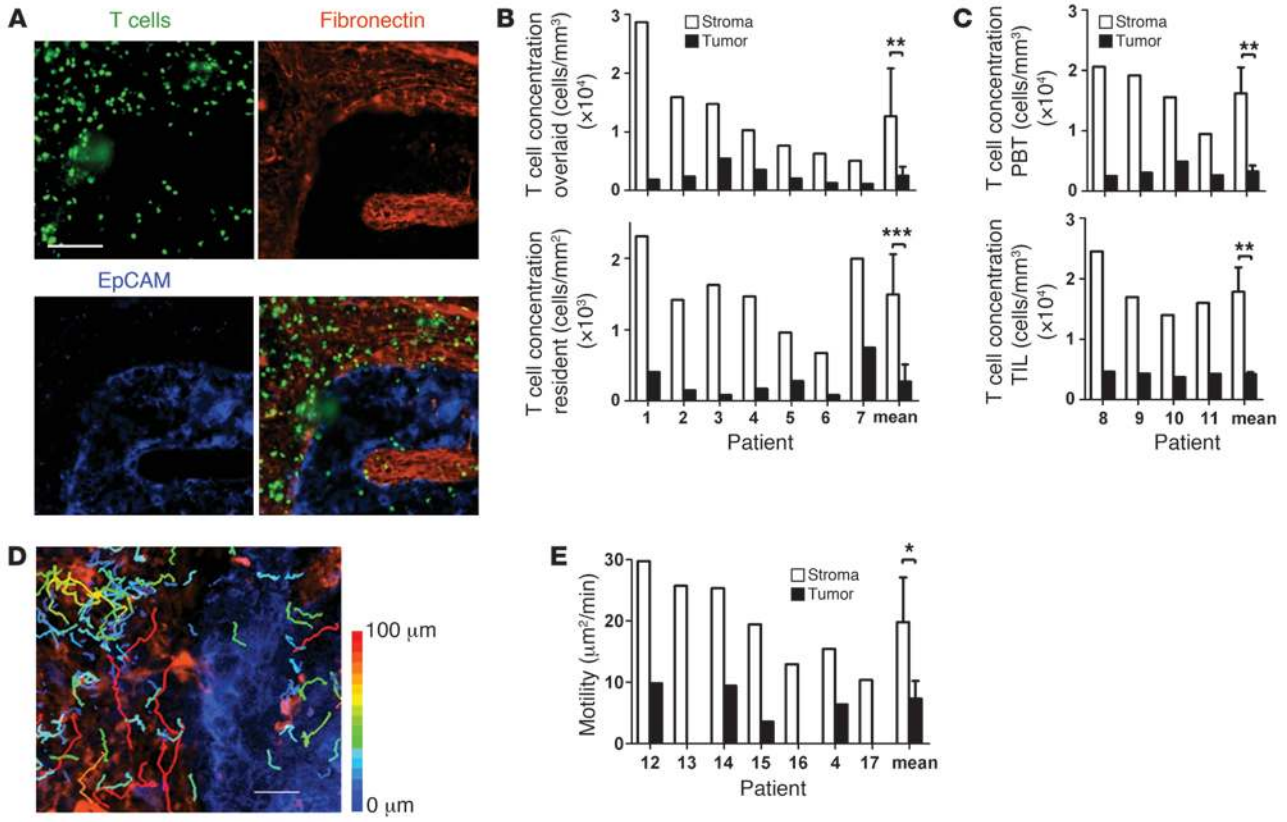

Figure 1

T cells preferentially migrate into the tumor stroma. (**A**) Preactivated T cells (Hoechst; green) were added to a human lung tumor slice that was subsequently stained for fibronectin and EpCAM to respectively identify stromal (red) and tumor epithelial cell (blue) regions. Each image, captured with a widefield microscope, is the maximum projection of 4 images spanning 60 μm in the *z* direction beneath the cut surface of the slice. (**B**) Concentration of in vitro activated T cells and resident $CD3^+$ cells in the stromal and tumor cell regions. (**C**) Concentration of in vitro activated PBTs and freshly isolated autologous TILs in the stromal and tumor cell regions. (**D**) Trajectories of individual T cells in the stromal (red) and tumor cell (blue) regions. Fluorescently labeled T cells introduced into a human tumor slice were imaged for 20 minutes, after which the slice was stained for fibronectin and EpCAM. Trajectories were superimposed over immunofluorescence images. Tracks are color coded according to extent of cell displacement. See also Supplemental Video 1. (**E**) Motility coefficient of T cells in the stromal and tumor cell regions. Values are mean ± SD of data obtained in slices from 7 (**B** and **E**) or 4 (**C**) different human lung tumors. $^*P < 0.05$; $^{**}P < 0.01$; $^{***}P < 0.001$. Scale bars: 100 μm (**A**); 50 μm (**D**).

found the stroma to be composed of several microenvironments in which T cell motility was either favored or restricted. These modes of migration were correlated with different patterns of ECM. In particular, we found that peritumoral ECM fibers played an important role in limiting T cell access to tumor cells.

Results

T cells accumulate and migrate preferentially in the stroma of human lung tumors. The overlay slice approach, initially set up in murine lymph nodes (9), was adapted to human lung tumors in order to dynamically visualize T cells in their native environment. A piece of a tumor rapidly obtained after tumor resection was embedded in agarose and then sliced with a vibratome. In vitro activated peripheral blood T cells (PBTs) and freshly isolated autologous tumor-infiltrating T lymphocytes (TILs), loaded with a fluorescent dye, were then immediately overlaid onto the slice. After 1 hour, T cells were imaged by collecting a series of images throughout a 60-μm depth, starting 10 μm below the cut surface, every 20 seconds for 20 minutes. Slices were then fixed and stained with fluorescent Abs in order to correlate the localization and migration of introduced T cells in relation to different tumor environments. Tumor cells were stained for epithelial cell adhesion molecule (EpCAM; an epithelial marker), whereas the stroma was stained for fibronectin (an abundant ECM protein) or CD90 (a surface protein expressed by several stromal cells, including fibroblasts and endothelial cells). A representative example of the T cell distribution in lung tumor slices is shown in Figure 1A. Plated T cells exhibited the same segregation as their resident counterparts and were preferentially recruited in the stroma, but rarely found in the tumor cell regions (Figure 1B). This uneven distribution was observed for both overlaid TILs and in vitro activated PBTs, with 5 times more T cells per volume unit infiltrated into the stroma than the tumor islets (Figure 1, B and C). There were no differences in the localization of $CD4^+$ and $CD8^+$ PBTs (Supplemental Figure 1; supplemental material available online with this article; doi:10.1172/JCI45817DS1). Notably, the preferential accumulation of T cells in the stroma was observed in all lung tumors, regardless of histological type, as well as in slices from a colon cancer patient (Supplemental Figure 2).

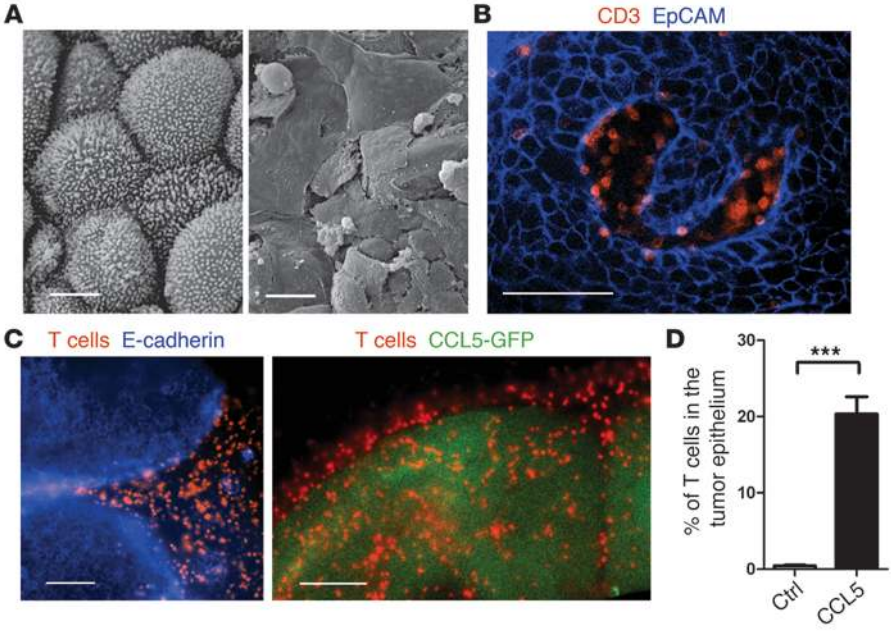

Figure 2

T cells are able to infiltrate tumor islets expressing CCL5. (**A**) SEM images of 2 different tumors from lung cancer patients, showing cohesive tumor cells. (**B**) Representative image of a human lung tumor slice stained for EpCAM (blue) and CD3 (red), demonstrating resident T cell exclusion from the compact tumor epithelium. (**C**) Fluorescently labeled T cells (Hoechst; red) from a tumor-specific clone were plated onto the slice of an autologous lung tumor engrafted into an immune-incompetent mouse. Tumor cells were identified by staining for E-cadherin (blue), or autologous tumor cells were transfected with a construct coding for CCL5-GFP (green) before their implantation. Images were captured as in Figure 1A. See also Supplemental Video 2. (**D**) Proportion of fluorescently labeled T cells in tumor cell regions expressing or lacking CCL5 compared with the stroma. Only cells localized 10 μm below the surface of the slice were included in the analysis. Values are mean ± SD of 5 experiments in which T cells were scored from at least 3 tumor slices. ***$P < 0.001$. Scale bars: 5 μm (**A**); 100 μm (**B** and **C**).

We then determined the motile behavior of introduced preactivated T cells into the stroma and tumor cell regions of slices from human lung tumors. The few T cells found in the tumor islets exhibited very limited displacement (Figure 1D and Supplemental Video 1). In contrast, T cells located in the stroma showed much better motility, but with large variations in the mode of displacement from one stromal region to another. The motility coefficient, an index of the volume scanned by T cells, was on average 3 times higher in the stroma than in the tumor epithelial compartment (Figure 1E).

The main features of our findings in human lung tumors were also confirmed in a xenograft system. This model allowed us to use a $CD8^+$ tumor-specific T cell clone derived from PBTs of a lung cancer patient (H32-22) as well as autologous tumors previously established from a tumor cell line engrafted in NOD-SCID immunodeficient mice (14, 15). In vitro, tumor-specific T cells were able to form conjugates with autologous tumor cells and exhibited antigen-dependent Ca^{2+} responses triggered by cell-cell interactions (14). However, when plated onto slices of the engrafted tumors, tumor-specific T cells accumulated in the stroma and not in the epithelial tumor cell region, stained for E-cadherin (Supplemental Figure 3). Thus, despite open access to both the stroma and the tumor mass via the cut surface of the slice, T cells accumulated and migrated preferentially into the peritumoral stroma.

Expression of a chemoattractant within tumor cell regions increases T cell recruitment. Physical parameters, such as the density of the tumor epithelial tissue, could provide an explanation for the low number of T cells found in these regions. Scanning electron microscopy (SEM) revealed that, despite marked variability in their morphology, cancer cells were tightly attached and formed cohesive tumor islets (Figure 2A). The tight apposition between tumor cells was also clearly visible after staining of their membranes with an anti-EpCAM Ab (Figure 2B). Compact islets were also observed in tumors formed in the xenograft model (data not shown). To determine whether tumor islets constitute an absolute barrier to T cell migration, we engineered the xenotransplanted tumors to express a chemokine and studied the specific capacity of T cells to infiltrate the carcinoma region. Human tumor cells were transduced with a construct coding for human CCL5 before their implantation into immune-incompetent mice. This chemokine was chosen because T cells from the H32-22 clone were previously shown to migrate well toward CCL5 in a transwell migration assay (15). We then used the slice assay to analyze the distribution and migration of T cells introduced into slices of tumors with and without expression of the chemokine. In the presence of CCL5, a significant fraction of T cells was found within the tumor cell regions (20.4%, versus 0.45% in the absence of CCL5; Figure 2, C and D). However, even in the presence of CCL5 in the tumor cell region, the number of T cells recruited into the stroma was still more pronounced. Analysis of motility parameters in both compartments revealed that T cells in tumor islets expressing CCL5 exhibited reduced speeds and straightness indices compared with cells in the stroma (Supplemental Figure 4 and Supplemental Video 2), indicative of a more confined migration. Moreover, stromal T cells surrounding the tumor islets did not migrate toward CCL5-expressing malignant cells, but displayed linear trajectories parallel to the tumor-stroma boundary, a mode of displacement we later analyzed in further detail in human tumors (see below). Together, these results indicated that tumor cell cohesion is not an absolute barrier to lymphocyte recruitment, since a fraction of T cells was able to infiltrate tumor nests expressing a chemoattractant. Moreover, our observations confirmed that the tumor stroma is a more favorable environment for attracting T cells.

Chemokines participate in recruitment and migration of T cells in some stromal areas of human lung tumors. Because chemokines are key factors for the exploratory behavior of T cells in lymphoid organs (8, 9), we next examined whether these molecules also control the migration of T lymphocytes in human lung tumors. We used pertussis toxin (PTX), a bacterial toxin that inhibits the GTP-binding proteins G_i and G_o and therefore blocks signaling from

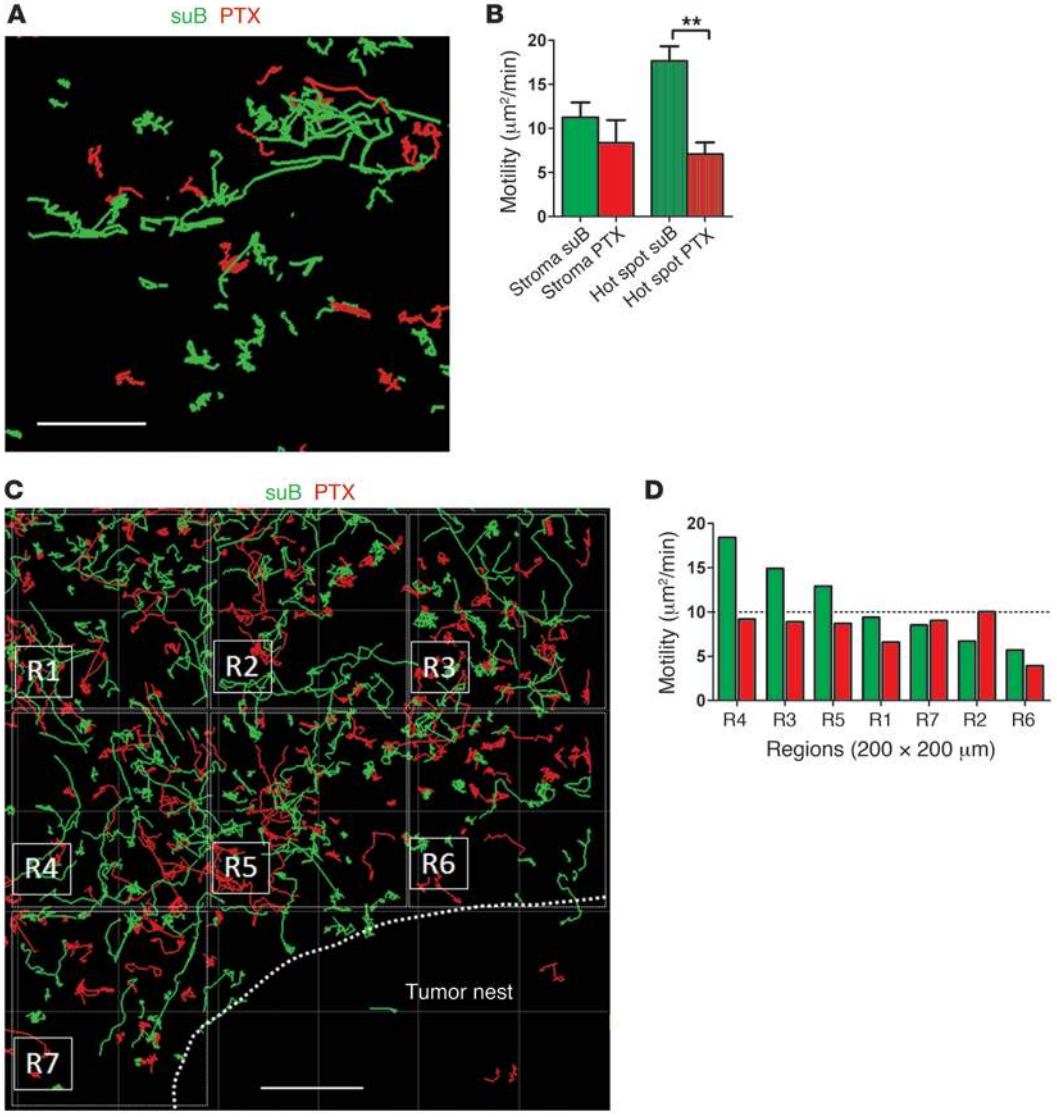

Figure 3

T cell migration within human lung tumor slices is partially inhibited by PTX. (**A**) Tracks of individual suB- (green) or PTX-treated (red) T cells in a human lung tumor slice during a 20-minute recording with a widefield microscope. T cells were incubated for 2 hours with 100 ng/ml suB or PTX, labeled with CMFDA and Hoechst, respectively, and overlaid on a tumor slice. Stroma was identified by staining for fibronectin (not shown). (**B**) Motility coefficient of suB- and PTX-treated T cells within the whole stroma and within hot spots, in which lymphocyte motility was favored (see **D**). Values are mean and SD from experiments performed on tumor slices from 5 different lung cancer patients. At least 100 cells were analyzed per experiment. (**C**) Tracks of individual suB- (green) and PTX-treated (red) T cells measured in a microscopic field of a human lung tumor slice during a 20-minute recording. 7 200-μm × 200-μm adjacent stromal regions (R1–R7) are indicated. (**D**) Motility coefficient of suB- and PTX-treated T cells analyzed within the 7 adjacent stromal regions in **C**. Dashed lines denote the 10-μm²/min threshold for hot spots. $^{**}P < 0.01$. Scale bars: 50 μm (**A**); 100 μm (**C**).

chemokine receptors and other G protein–coupled receptors. The inactive B subunit of PTX (suB) was used as a control. PTX- and suB-treated T cells, loaded with 2 different fluorescent dyes, were simultaneously imaged in slices from 5 different tumor specimens. Contrary to prior observations of naive T cells in murine lymph nodes (9), the number of PTX-treated T cells was only slightly reduced in the stroma of human lung tumors compared with that of control cells. However, PTX induced a 25% decrease in the average T cell motility measured in the stroma, although this was not statistically significant because of the large variability in T cell distribution and motilities (Figure 3, A and B). We next sought to determine the origin of this variability by analyzing the migration of T cells in adjacent 200-μm × 200-μm stromal regions (Figure 3C). As shown in Figure 3D, the motility coefficients calculated were highly variable from region to region. Promigratory regions in which motility coefficients exceeded 10 μm²/min covered on average 20% of the surface of the tumor stroma. Remarkably, we found that PTX partially but significantly inhibited the displacements of T cells only in these regions, which we termed *hot spots* (Figure 3B). Thus, chemokines participated in controlling

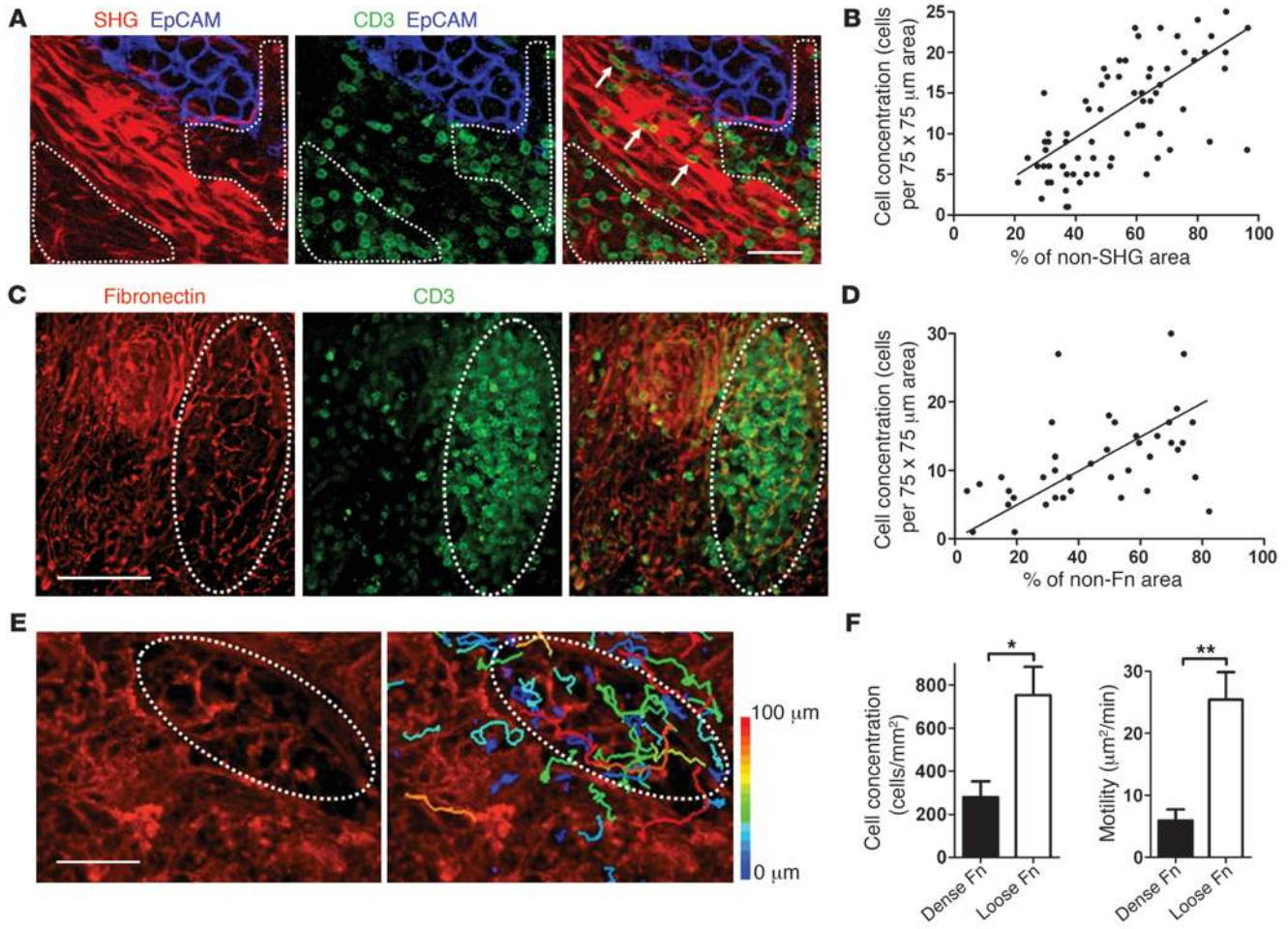

Figure 4

Matrix fiber density strongly influences the localization and migration of T cells. (**A**) SHG signal (red) from a human lung tumor slice also stained for CD3 (green) and EpCAM (blue), showing accumulation of resident T cells in collagen-sparse regions (dashed lines). Arrows denote elongated T cells positioned between collagen fibers. Images were captured with a 2-photon microscope. (**B**) Automatically scored number of resident T cells in 75-μm × 75-μm zones, showing percent SHG-free area (see Supplemental Figure 5). Results were obtained on slices from 3 different lung tumors. (**C**) Representative image of a human lung tumor slice stained for fibronectin (red) and CD3 (green). A fibronectin-sparse area enriched in T cells is shown (dashed outline). (**D**) Automatically scored number of resident T cells in adjacent 75-μm × 75-μm zones, showing percent fibronectin-free area. Results were obtained on slices from 5 different lung tumors. (**E**) Trajectories of individual T cells in a human tumor slice poststained for fibronectin during a 20-minute recording. Tracks are color coded according to extent of cell displacement. A stromal region characterized by a loose fibronectin network is shown (dashed outline). See also Supplemental Video 3. (**F**) Motility coefficient and concentration of fluorescently labeled T cells in dense and loose fibronectin regions. Values are mean and SD from experiments performed on slices from 6 different tumor specimens. *$P < 0.05$; **$P < 0.01$. Scale bars: 50 μm (**A**); 100 μm (**C** and **E**).

T cell migration in some stromal regions of human lung tumors, but the partial inhibitory effect of PTX revealed the involvement of other factors in T cell exploratory behavior.

T cell distribution and migration is influenced by the structure of the tumor stroma. We next sought to determine the role played by the ECM of the tumor stroma in T cell positioning and migration. We used 2-photon imaging and second harmonic generation (SHG) combined with immunostaining to visualize collagen and fibronectin structures on human lung tumor slices. SHG directly visualizes the type I collagen in the ECM without exogenous stains. Figure 4, A and C, clearly illustrate the heterogeneity of the stroma in terms of ECM structures and T cell distribution. Stromal regions enriched in lymphocytes were characterized by a loose network of collagen and fibronectin fibers. By systematically analyzing the number of resident T cells in adjacent 75-μm × 75-μm stromal areas (Supplemental Figure 5), we found that the cell concentration was directly correlated with the lack of ECM structures: stromal regions exhibiting dense accumulation of fibronectin or collagen were nearly devoid of T cells (Figure 4, B and D), and the few T cells found in these areas were positioned in the gaps between fibers. Notably, lymphocyte-rich areas were characterized by the presence of thin fibers showing an average spacing of 14.0 ± 0.45 μm (Supplemental Figure 6, A and B), a value close to that calculated in the T zone of human lymph nodes (16.3 ± 4.5 μm; Supplemental Figure 6, D and E) and to that previously described for murine lymph nodes (17.2 ± 6.9 μm; ref. 10). The number of T cells and the distance between fibers analyzed in the same regions were correlated (Supplemental Figure 6C). We then

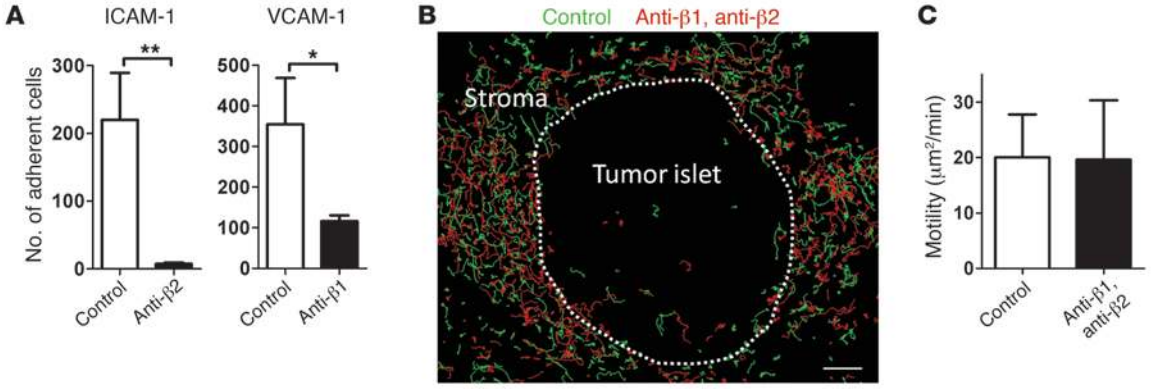

Figure 5

Blocking the interactions of β1 and β2 integrins with their ligands does not affect T cell migration in the stroma of human lung tumors. (**A**) Anti–β1 integrin and anti–β2 integrin Abs strongly inhibited adhesion of activated PBTs on VCAM-1 and ICAM-1. T cells pretreated or not with 10 μg/ml anti–β2 integrin mAb or anti–β1 integrin mAb were allowed to adhere on ICAM-1 or VCAM-1 layers for 10 minutes. After several washes, the number of remaining T cells was scored. Values are mean and SD from 3 different experiments. (**B**) Tracks of individual T cells treated (red) or not (green) with 10 μg/ml anti–β1 integrin and anti–β2 integrin mAbs in a human lung tumor slice during a 20-minute recording with a widefield microscope. (**C**) Motility coefficient of control and Ab-treated T cells within the tumor stroma. Values are mean and SD from experiments performed on tumor slices from 3 different lung cancer patients. At least 100 cells were analyzed per experiment. $*P < 0.05$; $**P < 0.01$. Scale bar: 100 μm.

performed dynamic imaging of T cells in human lung tumor slices that confirmed the negative effect of dense ECM on T cell accumulation and motility (Figure 4E and Supplemental Video 3). A typical example of T cells migrating within porous collagen structures, as visualized by 2-photon imaging, is illustrated in Supplemental Video 4. Analysis performed in slices from 6 different human lung tumors showed a lower concentration of T cells in these fibronectin-rich regions than in loose-fibronectin zones; similarly, the motility of T cells was greatly reduced in dense matrix regions (Figure 4F).

Apart from dense and porous areas, we also observed stromal regions in which fibronectin fibers were predominantly oriented in a single direction (Supplemental Figure 7). Most T cells exhibited linear tracks parallel to these organized fibers (Supplemental Figure 7B). It was not uncommon to see several cells migrating on a same track or a single cell migrating back and forth on the same path.

Blocking anti–β1 integrin and anti–β2 integrin Abs do not interfere with T cell migration within human lung tumor stroma. The T cell displacement along stromal matrix fibers prompted us to investigate the role played by adhesion molecules in these processes. β1 and β2 integrins are adhesion molecules that are expressed by activated T cells and bind to a variety of ligands, including ECM components such as collagen and fibronectin.

Blocking Abs were used to examine whether T cells use β1 and β2 integrins to migrate within the stroma of human lung tumors. We first performed in vitro experiments to test the capacity of these Abs to block the interaction of β1 and β2 integrins with their ligands. As shown in Supplemental Video 5, a substantial proportion of in vitro activated T cells spontaneously adhered and migrated on VCAM-1 and ICAM-1 layers. Notably, adhesion of T cells to these recombinant proteins was strongly inhibited by anti–β1 integrin Ab and by anti–β2 integrin Ab (Figure 5A). We then studied the effect of these Abs on the T cell exploratory behavior exhibited in human lung tumor slices. In contrast to the results in vitro, pretreatment of T cells with both β1 and β2 integrin Abs did not affect their accumulation into the stroma or their motility (Figure 5, B and C). Thus, T cells use β1 integrin– and β2 integrin–independent mechanisms for accumulation and migration within the stroma of human lung tumors.

T cells actively migrate along matrix fibers surrounding blood vessels. Organized and aligned ECM structures were mostly found either around blood vessels or at the tumor-stroma interface. To assess cell movement in perivascular regions of human lung tumor slices, fluorescently labeled T cells were added on slices, which were then further stained for fibronectin and CD31, an endothelial cell marker. Introduced T cells were more concentrated in regions surrounding blood vessels than in other stromal parts and migrated more actively in these perivascular regions, as evidenced by a higher motility coefficient (Figure 6, A and B). In perivascular regions, most of the T cells were found migrating in a linear manner along fibronectin fibers positioned parallel to the vessels (Figure 6C and Supplemental Videos 6 and 7). To quantify this motility pattern, we analyzed the trajectory vectors, the connecting lines between start and end points of each track. Measurement of the smallest angle between vector and vessel axis resulted in values substantially less than 45° (22.5° ± 19.5°; $n = 114$ cells; Figure 6D), whereas random migration would give values close to 45° on average. Moreover, observations of cross-sections revealed multiple layers of fibronectin fibers forming a concentric structure surrounding blood vessels (Figure 6E). In these perivascular regions, the average distance between fibronectin fibers, measured from immunofluorescent images, was 11.0 ± 2.9 μm (39 gap sizes analyzed from 3 different tumor specimens). SEM confirmed such patterns by revealing the presence of spaces between the layers (Figure 6F). In longitudinal sections, the ECM parallel strands were clearly visible. We concluded that perivascular regions, because of their particular loose and organized structures, are well suited to favor T cell trafficking along the vessels.

Matrix fibers surrounding tumor islets restrict T cell access to tumor cells. The presence of dense and parallel fibers of ECM was also observed in stromal regions immediately adjacent to tumor islets (Supplemental Figure 8A). Close examination of the few T cells found in these areas showed that resident lymphocytes displayed an elongated

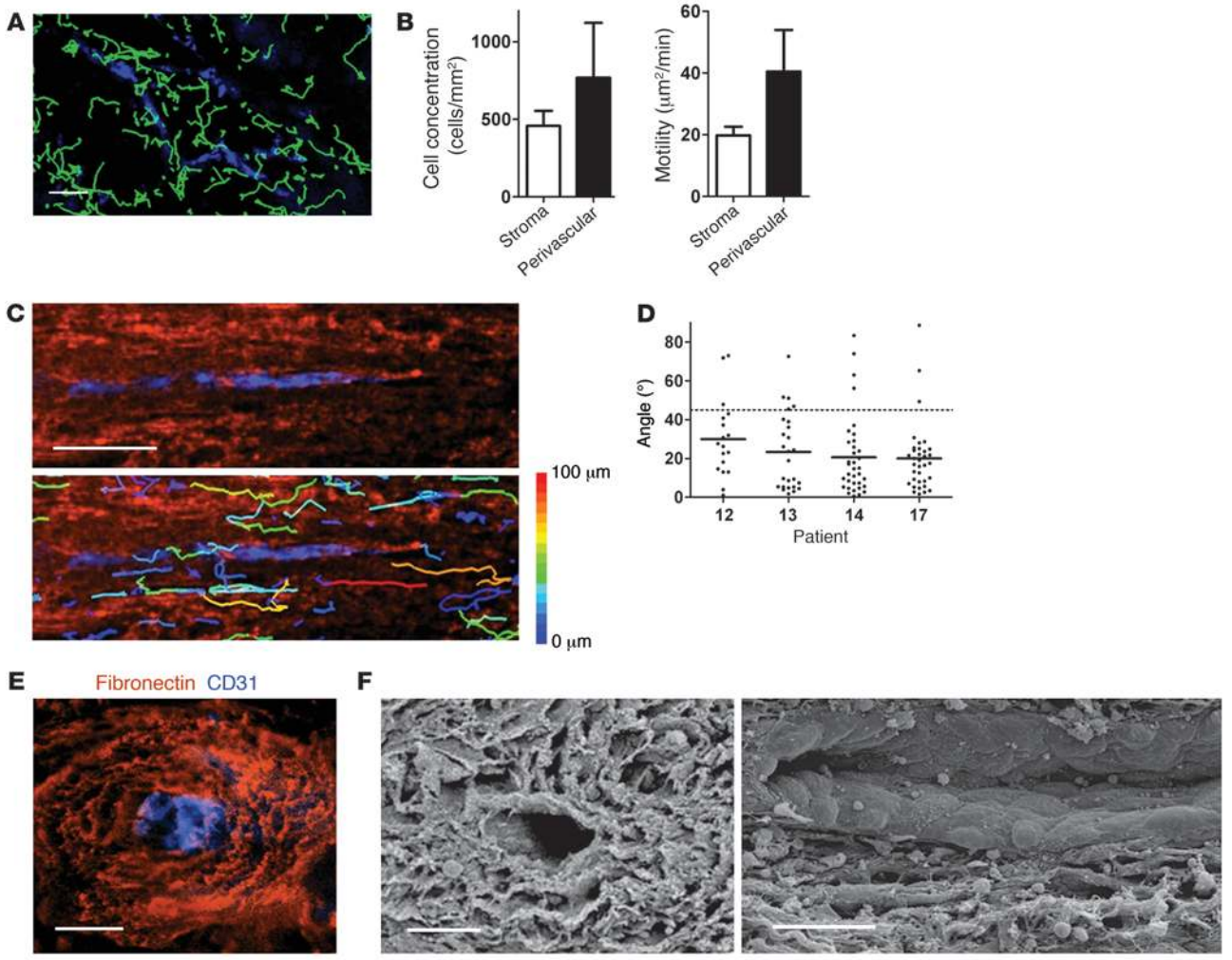

Figure 6

T cells actively migrate in perivascular regions of human lung tumors. (**A**) Individual T cell trajectories (Hoechst; green) in a human lung tumor slice poststained for CD31 to reveal blood vessels (blue), during a 20-minute recording with a widefield microscope. (**B**) Motility coefficient and density of T cells in the whole stroma and in perivascular stromal regions. Values are mean and SD from experiments performed on slices from 4–9 different human lung tumors. (**C**) Higher-magnification individual T cell trajectories in a human lung tumor slice poststained for fibronectin (red) and CD31 (blue) during a 20-minute recording. Tracks are color coded according to extent of cell displacement. Note the linear migration of T cells along fibers surrounding the vessel. See also Supplemental Video 7. (**D**) Angle between vessel axis and trajectory vector of individual T cells during a 20-minute recording, measured in slices from 4 different tumor specimens. Cells that migrated less than 10 μm were excluded from analysis. Dashed line denotes 45°, the expected result from a cell population migrating with no directional bias. (**E**) Representative image of a human lung tumor slice stained for fibronectin (red) and CD31 (blue), showing layers of fibers surrounding the blood vessel. (**F**) SEM cross-section (left) and longitudinal (right) images of human lung tumor slices, showing the outer layer of the vessel. Scale bars: 100 μm (**A** and **C**); 50 μm (**E** and **F**).

morphology along the linear fibers (Figure 7A). SEM confirmed the presence of linear strands parallel to the tumor-stroma interface (Figure 7B). To image T cells in stromal regions surrounding tumor islets, we stained human lung tumor slices containing introduced T lymphocytes for EpCAM and CD90. In stromal regions adjacent to tumor islets, most of the lymphocytes exhibited displacements parallel to the tumor-stroma boundary (Figure 7C). Accordingly, the angles between the displacement vectors and the tumor-stroma interface were less than 45° (Figure 7D). Quantification of the net displacement of T lymphocytes indicated that cells migrated preferentially along surfaces parallel to the tumor-stroma interface. Remarkably, the few T cells whose tracks were perpendicular to the tumor-stroma boundary migrated preferentially away from the tumor islets (16% versus 9%; Figure 7E). Differences in fiber density could be responsible for this directional bias: the gap size between fibrils was significantly smaller in regions immediately adjacent to the tumor-stroma boundary than that in regions 50 μm away from tumor islets (Figure 7F and Supplemental Figure 8B). To examine whether dense matrix fibers around tumor islets are responsible for the low ability of T cells to reach cancer cells, human lung tumor slices were incubated with bacterial collagenase. Treatment of tumor slices with 0.5 mg/ml collagenase for 30 minutes resulted in a marked decrease in stromal collagen content without substantial alteration in tumor architecture (Figure 8A). We then analyzed the consequences of collagenase treatment on the localization of overlaid T cells. Remarkably, instead of

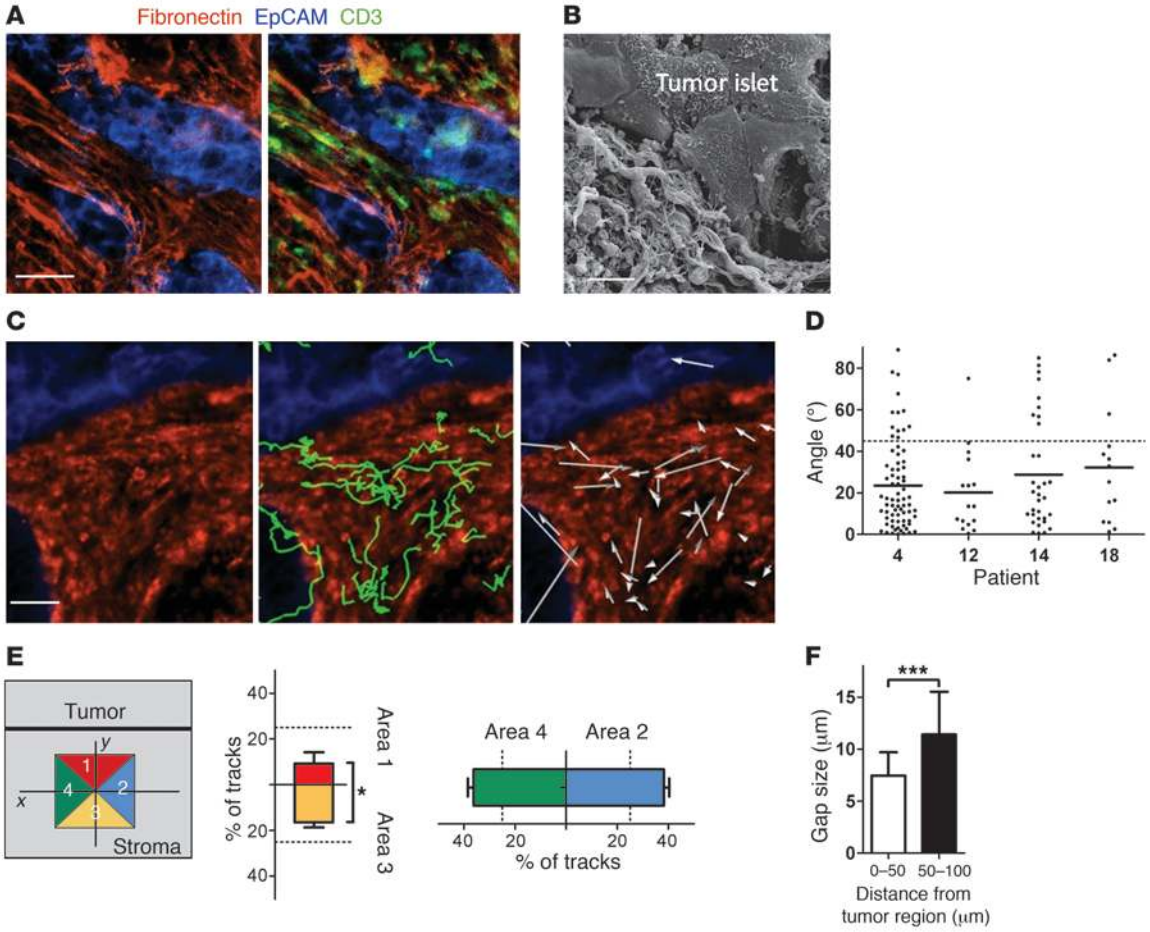

Figure 7

Matrix fibers surrounding tumor islets restrict T cells from contacting tumor cells. (**A**) Representative image of a human lung tumor slice stained for fibronectin (red), EpCAM (blue), and CD3 (green), demonstrating the presence of parallel fibers adjacent to the tumor cell regions. (**B**) Representative SEM image showing ECM strands parallel to the tumor cell regions. (**C**) Motility pattern of T cells (Hoechst; green) introduced into a human lung tumor slice stained for fibronectin (red) and EpCAM (blue). Also shown are tracks (middle) and trajectory vectors (right) during a 20-minute recording. (**D**) Angle between tumor-stroma boundary and trajectory vector of individual T cells, measured in tumor slices from 4 different lung cancer patients. Dashed line denotes 45°, the expected result from a cell population migrating with no directional bias. (**E**) Migration pattern of T cells in stromal regions adjacent to the tumor-stroma interface. Graphs represent the proportion of tracks whose end positions after the 20-minute recording were within each 90° segment (left scheme). The starting position of each cell was set at the *x*-*y* axis intersection, with the *x* axis parallel to the tumor-stroma boundary. Dashed lines denote 22.5°, the expected result from a cell population migrating with no directional bias. (**F**) Gap size between fibronectin fibers in 50-μm increments from the tumor islets. Values in **E** and **F** are mean and SD from experiments performed on tumor slices from 4 different lung cancer patients. ***$P < 0.001$. Scale bar: 50 μm (**A**); 10 μm (**B**); 100 μm (**C**).

being excluded from the immediate vicinity of cancer cells, overlaid T cells were uniformly localized in the stroma after collagenase treatment. This resulted in a 2-fold increase in the number of T cells in stromal regions immediately adjacent to tumor islets (Figure 8B). Furthermore, the number of T cells in contact with peripheral tumor cells was 2-fold larger in collagenase-treated than in control slices (Figure 8C). Overall, these results further demonstrated that the density and the disposition of the stromal ECM surrounding tumor islets dictate T cell migration behavior and restrict lymphocytes from contacting cancer cells.

Discussion

In the present work we have shown that, besides mechanisms of immunosuppression that have not been examined here, a key reason for the weak antitumoral efficiency of T lymphocytes in human cancers could be related to their location in tumor stroma, which impedes their direct contact with tumor cells. By combining immunostaining and real-time imaging of T cells introduced into fresh ex vivo human lung tumor slices, we demonstrated the presence of PTX-sensitive chemoattractants that favored T cell motility in some parts of the stroma, but not in tumor nests. However, in addition to this somewhat expected mechanism, we identified the existence of a PTX-insensitive component of T cell motility and demonstrated that although the cohesive structure of the tumor did not favor T cell recruitment, it did not constitute an absolute barrier for T cell infiltration. We also showed that the detailed organization of matrix fibers, namely their spacing and orientation, contributed to constraining T cell movement in the stroma. Finally, we described a dense collagen network surrounding tumor islets that limited T cell trafficking. Indeed, matrix

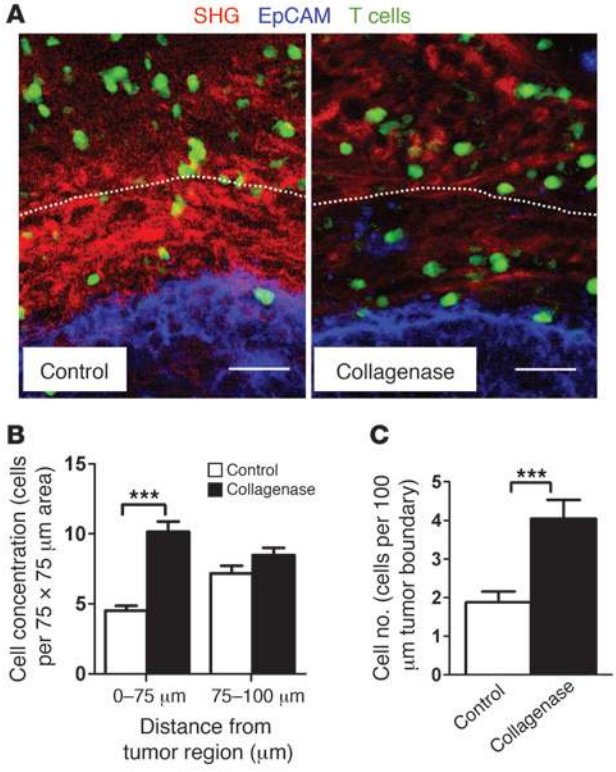

Figure 8
Collagenase enhances the number of T cells in contact with tumor cells. (**A**) Human lung tumor slices were treated or not with collagenase (0.5 mg/ml) for 30 minutes. In vitro activated PBTs loaded with a fluorescent dye (Hoechst; green) were added to the slices, which were subsequently stained for EpCAM (blue) to identify tumor cell regions. SHG (red) was used to visualize the collagen network. Each image, captured with a 2-photon microscope, is the maximum projection of 10 images spanning 100 μm in the *z* direction beneath the cut surface of the slice. Dotted white line denotes the first 75 μm of the stromal region adjacent to the tumor islet. (**B**) Number of T cells in 75-μm × 75-μm zones adjacent to tumor cell regions. (**C**) Number of T cells in contact with peripheral cancer cells along the tumor-stroma boundary. Values in **B** and **C** are mean and SD from experiments performed on tumor slices from 3 different lung cancer patients. ***$P < 0.001$. Scale bars: 50 μm.

loosening induced by collagenase treatment increased the ability of added T cells to contact tumor cells.

An important initial result in our experimental model was that exogenous T cells added to tumor slices migrated exactly in the regions where endogenous T lymphocytes were present, just as exogenous naive T cells were previously shown to migrate exclusively in T cell zones in lymph node slices (9). In the present study, we used preactivated rather than naive T cells, after verifying that activated T cells infiltrated tumor tissues much more efficiently that did resting T lymphocytes (Supplemental Figure 9).

We next examined whether the T cells' low capacity for tumor islet infiltration was simply caused by cell-cell junction tightness in tumor nests. Prior in vitro experiments performed in 3D collagen matrices show that T cells, like other cells that exhibit amoeboid migration, are able to adapt their morphology and even deform their nucleus in order to flow through narrow gaps (16, 17). However, prohibitive matrix density and the protease-independent nature of T cell migration forces lymphocytes to change their direction toward paths of least resistance, a process known as contact guidance (17). Our finding of substantial T cell recruitment in tumor islets expressing CCL5, a chemoattractant for activated T cells, suggests that T lymphocytes can overcome this structural constraint, at least in a xenograft system. Thus, even if the compactness of the tumor cell regions affects the recruitment of T cells, this physical barrier is not an absolute one. Rather, it is likely that the paucity of T cells in tumor epithelial compartments is also caused by other factors, such as lack of T cell retention and migration factors expressed by tumor cells. This is in line with our results showing altered expression of chemokines during the transformation process. Indeed, keratinocytes from human skin tumors exhibited reduced expression of CCL27, a potent attractor of T cells toward the skin (18). Apart from reduced expression during malignant transformation, intratumoral chemokines can also be modified by peroxynitrites, which leads to defective recruitment of T cells to tumor islets (19). In addition to chemokines, other migration cues can also be decreased in tumor nests. For instance, T cells do not bind to tumor cells from colorectal cancer, which suggests that upon tumorigenesis, colon epithelial cells lose adhesion molecules (20). Moreover, tumor cells could potentially express antimigratory factors for T cells, although this interesting possibility has not yet been properly explored. Finally, the lack of oxygen in tumor islets could also affect T cell migration, since this phenomenon has previously been shown to be strongly oxygen dependent (21, 22).

The paucity of T cells in carcinoma regions depended not only on tumor cells, but also on specific features of the host stroma. In particular, our data indicated that the organization of the matrix fibers at the cancer cell–stroma interface contributed to limiting T cell movement within the stroma. The stroma is an important component of most tumors, and its protumorigenic action has clearly been established (13). Tumor formation leads to host environment remodeling associated with activation of stromal fibroblasts, which synthesize multiple factors, including ECM proteins. It has previously been suggested that a tumor may be perceived by the organism as a permanent wound, with tissue damage triggering a healing process that may in turn favor tumor growth and metastasis (23). The structural feature we described here in lung tumors — dense parallel fibers adjacent to tumor islets — has also been observed in human melanoma and breast cancer metastases (24). In a mouse breast tumor model, collagen strands adjacent to tumor nests adopt several patterns during carcinoma progression, including similar ring structures around tumor cell regions that were observed at early stages of tumorigenesis (25). Yet to our knowledge, the role of stromal components in controlling T cell behavior has not previously been addressed. Recent 2-photon studies have shown that T cell migration is not a random process, but is controlled by environmental factors, including ECM fibers (8, 26, 27). In mouse tumor models, occasional T cell movements along collagen fibers have been described (28, 29). However, these studies have not addressed the location of these fibers in relation to the tumor cells and other stromal components. Another important point concerns the involvement of adhesion molecules in guiding T cells along ECM fibers. Using a blocking Ab approach, we found no effect of anti–β1 integrin and anti–β2 integrin on the accumulation and migration of T cells within the tumor stroma, whereas these Abs strongly inhibited adhesion of T cells to recombinant

ICAM-1 or VCAM-1 in 2D in vitro assays. Our results are in line with those obtained in 3D matrix, with activated T cells migrating independently of β1, β2, and β3 integrins (30). Accordingly, it has recently been proposed that T cells rely less on adhesive interaction and more on protrusive flowing of the actin cytoskeleton to migrate within a tissue (31).

The fresh tumor slice method enabled us to identify other stromal microenvironments that either favored or prevented T cell migration. Accumulation and active migration of T cells was observed in regions characterized by loose matrix fibers and sharing structural features with the reticular fiber networks of secondary lymphoid organs. The organization of the fibronectin fibers — in particular, the optimal spacing for guiding T cell movements — was quite comparable in both tissues, which may be due to similarities between their fibroblasts. Indeed, it has recently been shown that fibroblasts from mouse tumors express a gene set that promotes development of lymphoid-permissive tissue (32). In human lung tumors, lymphoid structures containing T cells, but also mature dendritic cells and proliferating B cells, have been described recently (33). Thus, providing tracks for active random migration and favoring ongoing immune responses would optimize efficient immune surveillance and antitumor immunity in these regions. Important molecular determinants of these lymphoid-like structures are chemokines able to recruit T cells and trigger their motility (34). Our data showed an inhibitory effect of PTX on T cell movement measured in promigratory regions of the stroma, which confirmed the participation of chemokines in these processes. Notably, the partial inhibitory effect of PTX is suggestive of participation of cues other than chemokines in the control of T cell localization and migration in some stromal regions. In vitro studies have shown that IL-2 was able to trigger cytoskeletal changes in activated T cells, but not in naive T cells (35). Whether cytokines participate in T cell trafficking in tumor stroma remains to be determined. Alternatively, intrinsic migratory behavior of preactivated T cells could also explain the relatively weak inhibitory effect of PTX. This would be consistent with our data showing basal locomotion of preactivated T cells that was amplified by chemokines contained within lymphoid-like structures of human lung tumors.

High numbers of T cells exhibiting active migration have been observed in perivascular regions of human lung tumor slices. In these regions, the stroma organization, parallel to the vessels, appears distinct from the loose and random organization of the lymphoid-like regions of the stroma. Different T cell subpopulations attracted by such structures have been previously reported. A fraction of migrating cytotoxic $CD8^+$ T cells was found to follow blood vessels during the late phase of tumor rejection in a tumor mouse model (28). Moreover, specific aggregates of $CD4^+$ T cells proximate to blood vessels have been observed in human glioblastoma, as well as in brains of patients or mice with autoimmune inflammation (36, 37).

In contrast to these favorable regions for T cell motiliy, dense expression of fibronectin and collagen was associated with a reduced ability of T cells to migrate and contact tumor cells, probably because of physical hindrance. Tumors are heterogeneous in terms of ECM textures (38). In human breast tumors, a high deposition of ECM proteins occurring during fibrosis is associated with a bad prognosis as a result of several mechanisms, including the promotion of metastasis (39). Moreover, experiments performed in animal models are indicative of extensive alterations of ECM proteins, including accumulation and stiffening, associated with tumor progression (40). Remarkably, murine breast tumors with a dense stroma were not eliminated as efficiently as tumors whose stroma had a looser appearance (41). Our present data, showing that matrix-rich regions around tumor islets acted as obstacles for T cell displacement and interaction with cancer cells, furnish a possible explanation for these results. In light of the present study, local action of antifibrotic molecules could be of clinical interest for facilitating T cell infiltration into tumor cell regions, thus improving the antitumor effect of immune cells.

To our knowledge, this is the first study to describe the dynamic behavior of T cells in a viable human tumor preparation. We identified a dense fibrous stroma around tumor islets that limited T cell access to cancer cells. The technique we developed may shed light on the gap that currently exists between results obtained in mouse models and those from fixed human samples. Although this system presents some limitations associated with the slicing, the possibility of culturing human tumor slices for up to 5 days while preserving the original cancer microenvironment (42) offers a number of promising applications. Increased understanding of the mechanisms by which this collagen network is generated has the potential to aid in the development of new therapeutics.

Methods

Human lung tumors. Fresh tumors from anonymized patients diagnosed with clinical stage I–III non–small cell lung cancer were rapidly transported to the laboratory in RPMI 1640 on ice. No chemotherapy or radiotherapy was administered before the operation. In total, 34 lung tumors were used for this study, of which 11 were discarded due to necrosis or a very high level of autofluorescence that precluded T cell imaging. Samples were categorized as having adenocarcinoma (41%), squamous cell carcinoma (35%), large cell carcinoma (12%), or mixed histological features (12%). For preliminary tests, some tumors were obtained from B. Terris (Hôpital Cochin, Paris, France) and A. Cazes (Hôpital européen Georges-Pompidou, Paris, France).

Human lung tumor xenografts were established as described previously (15). Briefly, tumor cells (IGR-Heu) from a lung tumor patient were engrafted subcutaneously into the flank of NOD-SCID mice. Tumors overexpressing CCL5 were obtained by infection of IGR-Heu cells with a lentivirus encoding human CCL5-IRES-GFP, followed by subcutaneous transplantation into NOD-SCID mice (15).

Cells and tumor slices. For TIL isolation, fresh biopsies were dissociated immediately after tumor resection. Single-cell suspensions were prepared by mechanical dissociation in RPMI without serum, filtered (100 μm) to remove membrane aggregates, and rinsed twice with PBS plus 5% FCS and 0.5 mM EDTA. TIL suspensions were isolated by Ficoll centrifugation (Ficoll-Paque Plus; Amersham Biosciences) followed by positive selection using CD4 and CD8 isolation kits (Miltenyi). Cells were then kept 2 hours in complete RPMI 1640 medium supplemented with 2 mM L-glutamine and 10% AB serum at 37°C, 5% CO_2 before the assay.

Human PBTs from healthy donors (Etablissement Français du Sang, Paris, France) were isolated by Ficoll gradient followed by negative selection using a T cell isolation kit (BD Biosciences). PBTs were stimulated with anti-CD3– and anti-CD28–coated beads at a 1:1 bead/cell ratio (Dynabeads; Invitrogen) in 96-round-well plates. Cells were cultured in complete RPMI 1640 medium supplemented with 2 mM L-glutamine and 10% AB serum (Cambrex). Recombinant IL-2 (30 U/ml; obtained from the NIH AIDS Reagent Program) was added at day 3. On day 6, beads were removed, and cells were transferred to 24-well plates. T cells were generally used for imaging experiments between days 8 and 15. As confirmed by flow cytometry, the T cell population showed a phenotype of effector cells, with CD45RO and CXCR3 expressed by more than 90% of

lymphocytes. The CD4/CD8 ratio was usually close to 1, with some variations observed among donors.

In some experiments, $CD4^+$ and $CD8^+$ T cells were isolated from in vitro activated PBTs by negative selection using either a CD4 or a CD8 isolation kit (Miltenyi).

The T cell clone (H32-22) specific for the IGR-Heu tumor cell line was established as described previously (14).

Tumor slices were prepared as described previously (9), with modifications. In brief, samples were embedded in 5% low-gelling-temperature agarose (type VII-A; Sigma-Aldrich) prepared in PBS. 400-μm slices were cut with a vibratome (VT 1000S; Leica) in a bath of ice-cold PBS. Slices were transferred to 0.4-μm organotypic culture inserts (Millicell; Millipore) in 35-mm Petri dishes containing 1 ml RPMI 1640 plus 10% AB serum in an incubator at 37°C, 5% CO_2. In some experiments, tissue sections were transferred to a 24-well plate with 1 ml/well RPMI 1640 supplemented with 0.5 mg/ml collagenase D from *Clostridium histolyticum* (Roche). Slices were incubated for 3 hours at 37°C, then rinsed in complete RPMI 1640 medium.

Cell preparation. Lymphocytes were stained with either 0.5 μg/ml Hoechst (Invitrogen) and 0.5 μM 5-chloromethylfluorescein diacetate (CMFDA; Invitrogen) for 5 minutes at 37°C or with 0.5 μM carboxylic acid acetate succinimidyl ester (SNARF; Invitrogen) for 20 minutes at 37°C in HBSS. Cells were washed in RPMI 1640 plus 10% AB serum and resuspended in this medium. In some experiments, T cells were pretreated for 2 hours with 100 ng/ml PTX or suB (Calbiochem) at 37°C and washed twice in RPMI 1640 plus 10% AB serum. 1.5×10^5 lymphocytes total in 10–20 μl were added onto the cut surface of each slice. To concentrate the cells on the slice, a stainless steel ring was placed on the agarose surrounding the tumor tissue. Slices were incubated for 1 hour at 37°C, 6% CO_2; gently washed to remove the residual cells that had not entered the tissue; and kept at 37°C, 6% CO_2 before imaging.

Time-lapse imaging. T cells were imaged with a widefield and a 2-photon microscope, both equipped with a chamber thermostated at 37°C. For imaging experiments performed with a widefield inverted microscope (Eclipse TE2000-U; Nikon), the preparation was placed upside-down on nylon threads glued to each of the extremities of a glass coverslip. In these conditions, the slice lies a few microns above the bottom of the dish, which facilitates renewal of the perfusion solution by bubbling with 95% O_2 and 5% CO_2. The preparation was perfused at a rate of 1 ml/min with RPMI without phenol red. Images were acquired with a ×4 (Plan fluor; Nikon) or ×10 (S fluor; Nikon) objective and MetaVue imaging software (Universal Imaging). For 4D analysis of cell migration, stacks of 4 sections (*z* step, 20 μm) were acquired every 20 seconds for 20 minutes at depths up to 60 μm. Imaging was usually done 10 μm below the cut surface of the slice. Videos were made by compressing the *z* information into a single plane with the best focus function of Metamorph. 2-photon imaging was performed with a DM500B upright microscope equipped with a SP5 confocal head (Leica Microsystems). Tumor slices were secured with a stainless steel washer and perfused with RPMI without phenol red bubbled with 95% O_2 and 5% CO_2. Excitation was provided by a Chameleon Ultra Ti:Sapphire laser (Coherent) tuned at 900 nm. Emitted fluorescence was split with a 560-nm dichroic mirror and passed through 465/30 (SHG), 525/50 (CMFDA), and 610/75 (SNARF) bandpass filters to non-descanned detectors. Images were acquired with a ×20 water immersion objective (×20/0.95 NA; Olympus).

In some experiments, T cells were incubated at 37°C with 10 μg/ml blocking anti–β1 integrin (4B4; Beckman Coulter) Ab and 10 μg/ml blocking anti–β2 integrin (7E4; Beckman Coulter) Ab for 20 minutes before the experiments.

For in vitro adhesion assay, glass coverslips were coated overnight at 4°C with 5 μg/ml human ICAM-1 Fc or VCAM-1 Fc (R&D Systems), washed with PBS, and blocked with PBS containing 1% BSA for 30 minutes at 37°C. T cells treated with blocking Abs and loaded with fluorescent dyes were left to adhere to ICAM-1 or VCAM-1 layers for 10 minutes at 37°C. Standardized washes were then applied to T cells: the medium was rapidly removed, and 2 ml prewarmed medium was added to the dish. The number of adherent T cells per microscopic field was then counted from processed fluorescent images.

Immunohistochemistry. Immunostainings were performed on slices previously fixed for 20 minutes with 2% paraformaldehyde. Slices were stained with the following primary Abs: mouse anti-CD3 (UCHT1; BD Biosciences), biotinylated mouse anti-EpCAM (R&D Systems), mouse anti-CD90 (5E10; BD Biosciences), mouse anti-CD31 (JC70A; Dako), and rabbit anti-fibronectin (Sigma-Aldrich). After 2–12 hours of staining at 4°C, slices were washed and incubated for 1 hour with the following Abs: Alexa Fluor 647–conjugated goat anti-rabbit IgG, Alexa Fluor 488–conjugated goat anti-mouse IgG (Invitrogen), and PE-conjugated streptavidin (BD Biosciences). All Abs were diluted in PBS with 0.5% BSA and 2% AB serum and used at a concentration of 10 μg/ml.

SEM. Tumor slices were fixed at room temperature with 4% prewarmed paraformaldehyde in PBS for 15 minutes. Samples were then washed, post-fixed in 1.5% osmium tetroxide, dehydrated in 5 successive and graded ethanol baths (from 25% to 100%), dried by the critical point method using liquid CO_2, coated with gold by sputtering, and observed with a scanning electron microscope (Cambridge Stereoscan 260).

Data analysis. Image analysis was performed at the Cochin Imaging Facility of Institut Cochin. Cellular motility parameters and cell numbers were calculated using Imaris 6.4 (Bitplane AG). Tracks in excess of 3 minutes were included in the analysis. The motility coefficient, a measure of the ability of a cell to move away from its starting position, was calculated by linear regression of squared displacement versus time. The straightness value was calculated as the ratio of the distance from origin to the total distance traveled. To reveal the relationship between cell motility and tumor structure, time-lapse images of T cells were superimposed onto the corresponding immunofluorescence images. Landmarks from the transmission light images helped us to find the corresponding regions.

The number of introduced lymphocytes was calculated within 3D volumes. Only cells localized 10 μm below the surface of the slice were included in the analysis. The concentration of resident $CD3^+$ T cells was determined within 2D surfaces, as Abs only stain the superficial region of the slice.

Angles between cell trajectory vectors (the connecting lines between start and end points of each track) and axes of blood vessels or tumor-stroma boundaries were calculated using Image J software. Only the cells positioned below a maximum distance of 100 μm from the vessels or tumor-stroma interfaces were included in further analysis.

Distances between fibronectin fibers were determined by using the line scan function of Metamorph.

T cell concentration and motility were quantified in different stromal environments, namely, dense vs. loose fibronectin regions and perivascular areas. These regions were identified by visual inspection of immunofluorescence images. Hot spots were identified by analyzing the motility coefficients of T cells in 200-μm × 200-μm stromal regions; regions with mean values larger than 10 μm^2/min were considered hot spots.

The relationship between T cell number and matrix density in defined 200-μm × 200-μm regions was quantified using Metamorph. First, fluorescent images were thresholded and converted to binary images. The Integrated Morphometry Analysis module was used to automatically count the number of T cells and calculate the percentage of the areas not filled by matrix components.

3D reconstruction of sequential *z* series were performed using Imaris.

Statistics. Statistical analysis was carried out using Prism (GraphPad Software). Significant differences between 2 series of results were assessed

using the unpaired 2-tailed Student's *t* test. A *P* value less than 0.05 was considered significant. Averages are expressed as mean ± SD.

Study approval. Human tumors were obtained with the agreement of the French ethic committee (no. 2008-133) and the AP-HP in accordance with article L.1121-1 of French law. Written informed consent was obtained from the patients prior to inclusion in the study.

Acknowledgments

We thank Pierre Bourdoncle and Camille Debugle (Cochin Imaging Facility, Institut Cochin) for advice and assistance with microscopes and help in data analysis; Virginie Garnier for assistance with SEM; Audrey Mansuet-Lupo and Marco Alifano for expertise in human lung tumors; and Nadège Bercovici, François Asperti-Boursin, and Georges Bismuth for valuable discussions and critical reading of the manuscript. This work was supported by grants from CNRS, INSERM, the Ligue Nationale Contre le Cancer, the Institut National Contre le Cancer, and the Ministère de l'Education Nationale et de la Recherche.

Received for publication July 8, 2011, and accepted in revised form December 14, 2011.

Address correspondence to: Emmanuel Donnadieu, Département d'Immunologie et d'Hématologie, Institut Cochin, 22 Rue Méchain, 75014 Paris, France. Phone: 33.1.40.51.65.64; Fax: 33.1.40.51.65.55; E-mail: emmanuel.donnnadieu@inserm.fr.

1. Frey AB, Monu N. Signaling defects in anti-tumor T cells. *Immunol Rev*. 2008;222(1):192–205.
2. Gajewski TF, et al. Immune resistance orchestrated by the tumor microenvironment. *Immunol Rev*. 2006;213(1):131–145.
3. Chen Q, Wang WC, Evans SS. Tumor microvasculature as a barrier to antitumor immunity. *Cancer Immunol Immunother*. 2003;52(11):670–679.
4. Clark RA, et al. Human squamous cell carcinomas evade the immune response by down-regulation of vascular E-selectin and recruitment of regulatory T cells. *J Exp Med*. 2008;205(10):2221–2234.
5. Ohtani H. Focus on TILs: prognostic significance of tumor infiltrating lymphocytes in human colorectal cancer. *Cancer Immun*. 2007;7:4.
6. Verdegaal EM, et al. Functional CD8+ T cells infiltrate into nonsmall cell lung carcinoma. *Cancer Immunol Immunother*. 2007;56(5):587–600.
7. Wakabayashi O, et al. CD4+ T cells in cancer stroma, not CD8+ T cells in cancer cell nests, are associated with favorable prognosis in human non-small cell lung cancers. *Cancer Sci*. 2003;94(11):1003–1009.
8. Mrass P, Petravic J, Davenport MP, Weninger W. Cell-autonomous and environmental contributions to the interstitial migration of T cells. *Semin Immunopathol*. 2010;32(3):257–274.
9. Asperti-Boursin F, Real E, Bismuth G, Trautmann A, Donnadieu E. CCR7 ligands control basal T cell motility within lymph node slices in a phosphoinositide 3-kinase-independent manner. *J Exp Med*. 2007;204(5):1167–1179.
10. Bajenoff M, et al. Stromal cell networks regulate lymphocyte entry, migration, and territoriality in lymph nodes. *Immunity*. 2006;25(6):989–1001.
11. Hojo S, et al. High-level expression of chemokine CXCL16 by tumor cells correlates with a good prognosis and increased tumor-infiltrating lymphocytes in colorectal cancer. *Cancer Res*. 2007; 67(10):4725–4731.
12. Harlin H, et al. Chemokine expression in melanoma metastases associated with CD8+ T-cell recruitment. *Cancer Res*. 2009;69(7):3077–3085.
13. Tlsty TD, Coussens LM. Tumor stroma and regulation of cancer development. *Annu Rev Pathol*. 2006;1(1):119–150.
14. Dorothee G, et al. In situ sensory adaptation of tumor-infiltrating T lymphocytes to peptide-MHC levels elicits strong antitumor reactivity. *J Immunol*. 2005;174(11):6888–6897.
15. Franciszkiewicz K, et al. Intratumoral induction of CD103 triggers tumor-specific CTL function and CCR5-dependent T-cell retention. *Cancer Res*. 2009;69(15):6249–6255.
16. Friedl P, Wolf K. Plasticity of cell migration: a multiscale tuning model. *J Cell Biol*. 2010;188(1):11–19.
17. Wolf K, Muller R, Borgmann S, Brocker EB, Friedl P. Amoeboid shape change and contact guidance: T-lymphocyte crawling through fibrillar collagen is independent of matrix remodeling by MMPs and other proteases. *Blood*. 2003;102(9):3262–3269.
18. Pivarcsi A, et al. Tumor immune escape by the loss of homeostatic chemokine expression. *Proc Natl Acad Sci U S A*. 2007;104(48):19055–19060.
19. Molon B, et al. Chemokine nitration prevents intratumoral infiltration of antigen-specific T cells. *J Exp Med*. 2011;208(10):1949–1962.
20. Kruger K, Buning C, Schriever F. Activated T lymphocytes bind in situ to stromal tissue of colon carcinoma but lack adhesion to tumor cells. *Eur J Immunol*. 2001;31(1):138–145.
21. Egeblad M, et al. Visualizing stromal cell dynamics in different tumor microenvironments by spinning disk confocal microscopy. *Dis Model Mech*. 2008;1(2–3):155–167; discussion 165.
22. Huang JH, et al. Requirements for T lymphocyte migration in explanted lymph nodes. *J Immunol*. 2007;178(12):7747–7755.
23. Cukierman E, Bassi DE. Physico-mechanical aspects of extracellular matrix influences on tumorigenic behaviors. *Semin Cancer Biol*. 2010;20(3):139–145.
24. Soikkeli J, et al. Metastatic outgrowth encompasses COL-I, FN1, and POSTN up-regulation and assembly to fibrillar networks regulating cell adhesion, migration, and growth. *Am J Pathol*. 2010; 177(1):387–403.
25. Provenzano PP, Eliceiri KW, Campbell JM, Inman DR, White JG, Keely PJ. Collagen reorganization at the tumor-stromal interface facilitates local invasion. *BMC Med*. 2006;4(1):38.
26. Matheu MP, et al. Imaging of effector memory T cells during a delayed-type hypersensitivity reaction and suppression by Kv1.3 channel block. *Immunity*. 2008;29(4):602–614.
27. Wilson EH, et al. Behavior of parasite-specific effector CD8+ T cells in the brain and visualization of a kinesis-associated system of reticular fibers. *Immunity*. 2009;30(2):300–311.
28. Boissonnas A, Fetler L, Zeelenberg IS, Hugues S, Amigorena S. In vivo imaging of cytotoxic T cell infiltration and elimination of a solid tumor. *J Exp Med*. 2007;204(2):345–356.
29. Mrass P, et al. Random migration precedes stable target cell interactions of tumor-infiltrating T cells. *J Exp Med*. 2006;203(12):2749–2761.
30. Friedl P, Entschladen F, Conrad C, Niggemann B, Zanker KS. CD4+ T lymphocytes migrating in three-dimensional collagen lattices lack focal adhesions and utilize beta1 integrin-independent strategies for polarization, interaction with collagen fibers and locomotion. *Eur J Immunol*. 1998;28(8):2331–2343.
31. Sixt M. Interstitial locomotion of leukocytes. *Immunol Lett*. 2011;138(1):32–34.
32. Peduto L, et al. Inflammation recapitulates the ontogeny of lymphoid stromal cells. *J Immunol*. 2009;182(9):5789–5799.
33. Dieu-Nosjean MC, et al. Long-term survival for patients with non-small-cell lung cancer with intratumoral lymphoid structures. *J Clin Oncol*. 2008;26(27):4410–4417.
34. de Chaisemartin L, et al. Characterization of chemokines and adhesion molecules associated with T cell presence in tertiary lymphoid structures in human lung cancer. *Cancer Res*. 2011;71(20):6391–6399.
35. Arrieumerlou C, et al. Involvement of phosphoinositide 3-kinase and Rac in membrane ruffling induced by IL-2 in T cells. *Eur J Immunol*. 1998; 28(6):1877–1885.
36. Barcia C Jr, Gomez A, Gallego-Sanchez JM, Perez-Valles A, Castro MG, Lowenstein PR, Barcia C Sr, Herrero MT. Infiltrating CTLs in human glioblastoma establish immunological synapses with tumorigenic cells. *Am J Pathol*. 2009;175(2):786–798.
37. Siffrin V, et al. Differential immune cell dynamics in the CNS cause CD4+ T cell compartmentalization. *Brain*. 2009;132(Pt 5):1247–1258.
38. Wolf K, et al. Collagen-based cell migration models in vitro and in vivo. *Semin Cell Dev Biol*. 2009; 20(8):931–941.
39. Hasebe T, Sasaki S, Imoto S, Mukai K, Yokose T, Ochiai A. Prognostic significance of fibrotic focus in invasive ductal carcinoma of the breast: a prospective observational study. *Mod Pathol*. 2002; 15(5):502–516.
40. Levental KR, et al. Matrix crosslinking forces tumor progression by enhancing integrin signaling. *Cell*. 2009;139(5):891–906.
41. Martin ML, et al. Density of tumour stroma is correlated to outcome after adoptive transfer of CD4+ and CD8+ T cells in a murine mammary carcinoma model. *Breast Cancer Res Treat*. 2010;121(3):753–763.
42. Vaira V, et al. Preclinical model of organotypic culture for pharmacodynamic profiling of human tumors. *Proc Natl Acad Sci U S A*. 2010;107(18):8352–8356.